Graphene interlayer for enhanced interface thermal conductance in metal matrix composites: An approach beyond surface metallization and matrix alloying

Huaijie Cao, Zhanqiu Tan, Ming-Hui Lu, G Ji, Xue-Jun Yan, Chen Di, Mengying Yuan, Qiang Guo, Yishi Su, Ahmed Addad, et al.

Graphene Interlayer for Enhanced Interface Thermal Conductance in Metal Matrix Composites: An Approach beyond Surface Metallization and Matrix Alloying

Huaijie Cao[a], Zhanqiu Tan[a], Ming-Hui Lu[b,c], Gang Ji[d], Xue-Jun Yan[b], Chen Di[b], Mengying Yuan[a], Qiang Guo[a], Yishi Su[a], Ahmed Addad[d], Zhiqiang Li[a], Ding-Bang Xiong[a, *]

[a]State Key Laboratory of Metal Matrix Composites, Shanghai Jiao Tong University, Shanghai 200240, China

[b]National Laboratory of Solid State Microstructures & Department of Materials Science and Engineering, College of Engineering and Applied Sciences, Nanjing University, Nanjing 210093, China

[c]Collaborative Innovation Center of Advanced Microstructures, Nanjing University, Nanjing 210093, China

[d]Unité Matériaux et Transformations (UMET) CNRS UMR 8207, Université de Lille, 59655, Villeneuve d'Ascq, France

Corresponding Author

* Ding-Bang Xiong: E-mail, xiongdingbang@sjtu.edu.cn;

Abstract

Poor wettability and acoustic mismatch between diamond and copper cause low interface thermal conductance and thus low thermal conductivity in their composites. In this work, beyond widely used strategies such as surface metallization and matrix alloying, in-situ grown graphene is introduced as a highly effective interlayer. The positive role of graphene on improving wetting between diamond and copper was supported by the increase of relative density, fractured surface morphology and interface microstructure. Thanks to the improved wetting and mitigated acoustic mismatch between diamond and copper, the interfacial thermal conductance is increased by ~3.7 times in the diamond/graphene/copper composite as indicated by differential effective medium calculation. Such a positive role of graphene

interlayer also agrees with the results from the time-domain thermoreflectance measurements. As a result, the thermal conductivity of the diamond/graphene/copper composite is 61% higher than that of the counterpart without graphene interlayer. This study provides a new approach for interface modification by 2D materials for a high TC of diamond/copper composite beyond surface metallization and matrix alloying.

Keywords: thermal conductivity; interface modification; diamond; graphene; copper

1. Introduction

Miniaturization of electronic components has led to an increase of power density in electronic devices, which calls for high thermal conductivity (TC) of thermal management materials to ensure heat dissipation **[1-3]**. Diamond/copper (Dia/Cu) matrix composites are considered as the latest generation of advanced materials for thermal management, owing to a high intrinsic thermal conductivity (up to 2000W/mK) **[4, 5]** and a low thermal expansion coefficient **[6]** of diamond along with a high working temperature of Cu. However, the fact of poor wettability **[7]** and weak (no chemical) bonding between the Cu and diamond makes it difficult to achieve effective combination and to improve the TCs of Dia/Cu composites **[8, 9]**. Furthermore, acoustic impedance ($Z = \rho v$, where ρ is density and v refers to phonon velocity, Z_{Cu} is 24.93×10^6 kg/m^{2}s, $Z_{Diamond}$ is 47.27×10^6 kg/m^{2}s) **[8]** mismatch between diamond and Cu leads to a low interfacial thermal conductance (ITC) and limits the improvement of TC.

Therefore, two main approaches have been developed for solving this problem. Metal matrix alloying (CuX, X = B, Cr, Ti) **[10-13]** is adopted to improve the interface bonding, while CuX alloys acted as matrix possess lower TCs than Cu matrix **[14]** because of the increase of stronger scattering center. Surface metallization of diamond particles **[15-17]** with a carbide forming element (W, Cr, Zr, B, Cu, Mo) is another way to enhance the TCs of Dia/Cu composites. With addition of a carbide forming element, a carbide interlayer would be formed to improve the interface bonding and wettability **[18]** under high temperature.

Moreover, the metallic carbide interlayers with appropriate acoustic impedance ($Z_{Cu} < Z_{carbide} < Z_{Diamond}$) act as a bridge to mitigate the acoustic mismatch between Cu and diamond **[8]**. But it still remains challenging in controlling the carbide interlayer since nano-sized thickness and uniform distribution are difficult to obtain by surface metallization. Preferential bonding of carbide forming elements on some crystal faces of diamond particle **[12, 19-23]** leads to thick and nonuniform carbide interlayers in final composite in order to achieve overall coverage on diamond's surface. However, too thick carbide layers with low TCs **[14]** decrease the TC of composite **[24]**. Moreover, it is hard to regulate composition of carbide interlayers, while the coexistence of carbide forming elements and as-formed carbides usually degrades ITC **[8]**. Additionally, interfacial action and the formation of carbides (such as Al_4C_3 in carbon/Al matrix composites) would result in a thick carbide interlayer and degrade the mechanical properties **[25, 26]** .

In this study, we propose that graphene acts as a highly effective interlayer between Cu matrix and diamond for enhancing the ITC and TC of Dia/Cu composites. Although graphene has a high in plane TC (3000-5000 W/mK) **[27]**, it (not graphite nanoplates) shows no enhancing effect on the TC of Gr/Cu composites according to the previous research **[28]**. Here, a strategy of in-situ grown graphene is proposed for interface modification because of the following three reasons. Firstly, in-situ catalytic growth of graphene on the starting Cu particle surface can avoid the problem of poor wettability between carbon and Cu and provide a strong bonding between Cu and graphene **[29, 30]**, and also graphene has a good compatibility with its allotrope of diamond because they have a closed specific surface energy **[31-33]**. Secondly, pristine graphene possesses an intermediate acoustic impedance (Z) of 42.04×10^6 Kg/m^{2}s **[34]**, which is analogous to metallic carbide. Defects and stress can decrease phonon velocity of graphene **[35-37]**, and thus the Z of the in-situ grown graphene is less than 42.04×10^6 kg/m^{2}s. Thirdly, compared to the aforementioned methods, uniform nanolayer of graphene can be easily obtained by decomposing the PMMA coated Cu, and the

thickness is tunable by adjusting the concentration of carbon source. Therefore, the in-situ grown graphene improves the interfacial wetting and bridges acoustic mismatch between diamond and Cu, thereby increasing ITC by ~3.7 times and contributing to the high TC (572.9 W/mK) of the as-produced 50 vol.% diamond/graphene/copper (Dia/Gr/Cu) composites.

2. Experimental Section

2.1. Materials

Spherical copper powders and poly-methyl methacrylate (PMMA) (M.W. 35000) were purchase from Alfa Aesar Chemical Co., Ltd, China. Absolute ethanol and anisole were obtained from Sinopharm Chemical Reagent Co., Ltd, China. Synthetic diamond (Type HWD40) of 70/80 mesh in size (180-210μm) and synthetic single-crystalline diamond plates (type HSCD 11) was purchased from Henan Huanghe Whirlwind Co., Ltd, China. The used material properties of diamond, copper and in situ grown graphene are shown in **Table 1**.

Table 1 The used Material properties of diamond, diamond plates, copper and in situ grown graphene.

Materials	Size	TC (W/mK)
Diamond	180-210μm	1600
Diamond plates	4×4×1 mm	1676
Copper	100-150μm	380
Graphene	3-4 μm (lateral dimension)	600-800 (an assumed in plane value)

2.2. Preparation of Dia/Gr/Cu Composites

The in-situ growth of graphene on spherical Cu powders was reported in our previous work **[28, 38]**. The spherical copper powders were annealed and reduced at 5% H_2/Ar atmosphere at 723 K. Then 30 g annealed Cu powders were added into 250 mL 0.08-0.25 wt% PMMA-anisole solution with stirring for 12 h. The mixtures were centrifuged at 4000

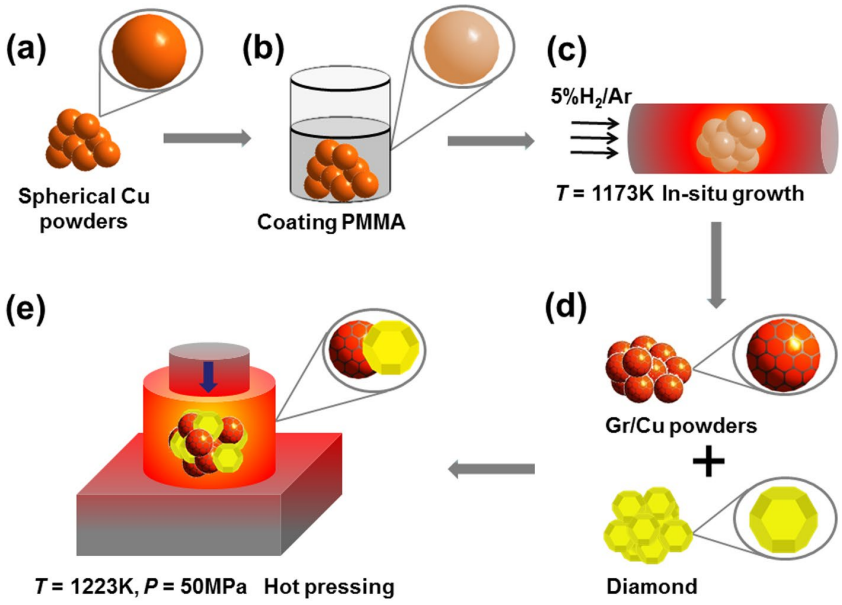

Fig. 1. Schematic illustration of preparation process of Dia/Gr/Cu composites.

rpm for 7 min. After that, the PMMA coated Cu powders were dried in a vacuum oven at 343 K for 12 h to remove the residual solvent. The dried PMMA/Cu powders were heated rapidly to 1173 K in tube furnace under the 5% H_2/Ar atmosphere at a heating rate of 10K/min. The temperature was kept for one hour. Finally, Gr/Cu composited powders were obtained by fast-cooling to room temperature. The 50 vol.% diamond particles and the as-prepared Gr/Cu composited powders were mixed and then densely stacked when loaded into a graphite die (Ø 12.7 mm). The powders were heated up to 1223 K in vacuum at a heating rate of 15 K/min and sintered at the temperature under a pressure of 50 MPa for 2 h. For comparison, the Cu and Dia/Cu samples without graphene were prepared by the same method. The whole preparation process is shown in **Fig. 1.**

2.3. Preparation of model material (Dia/Gr/Cu) for ITC measurement

Synthetic single-crystalline diamond plates (type HSCD 11, size:4×4×1 mm) were used as the substrate. To reduce their surface roughness, the diamond plates were successively polished by using the suspensions of diamond particles with a size of 9, 3 and 1 μm, and then were ultrasonically cleaned in acetone, ethanol and deionized water, and were bombarded for ~10 min by Ar ions. Prior to magnetron sputtering deposition, ~10 layers of graphene (to

simulate the condition for multi-layers graphene in bulk Dia/Gr/Cu composite) was transferred on the treated diamond substrate. RF magnetron sputtering (SPC300, USA) was applied to deposit Cu layer onto the transferred graphene. The sandwiched sample was denoted as Dia/Gr/Cu model materials and used for ITC measurements. The parameters of magnetron sputtering are listed in **Table S1** (Supporting Information). The thickness of deposited Cu film was measrued by SEM and the deposition rate was calculated to be 15 nm/min. The preparation process was shown in Fig. S1 (Supporting Information).

2.4. Characterization

The microstructures of the composite powders and bulk composites were examined by using scanning electron microscope (SEM, Mira3, acceleration voltages was 5 KV) and transmission microscope (TEM) (JEOL JEM-2100F, acceleration voltages was 200 KV). The content of impurities in the raw Cu powder was analysed by an Inductively Coupled Plasma Optical Emission Spectrometer (ICP-OES, Thermo Electron, USA). Energy-dispersive X-ray spectroscopy (EDS, acceleration voltages was 20KV) was used for elemental analysis. Raman spectra of diamond and graphene were collected by using Ar+ laser with a wavelength of 532 nm (spot size 1 μm and laser power 5 mW) as excitation source (Bruker Optics Senterra R200-L). Grating was 1800 g/mm, the objective magnification was 100 times, and integration time was 10 second. X-Ray diffraction (XRD) test was performed on a Rigaku D/max2550VL/PC system with Cu K_α radiation. Nitrogen concentration of the diamond was analyzed by Microscopes Fourier transform infrared spectra (Micro FTIR, NicoletiN10 MX, USA). During the test, the infrared beam grating was controlled at 150 μm so that the beam passes through only one plane of a single diamond particle. The spectral test range was 700~4000 cm^{-1}. Atomic force microscope (AFM, Bruker, Germany) was used to characterize the surface morphology of single crystalline diamond plates. A focused ion beam (FIB) system (FEI, Nova 200, USA, acceleration voltages was 30 KV) was used to prepare the Dia/Gr/Cu TEM sample. The rough surface of Dia/Gr/Cu composite was mechanical polished

and then milled by surface ion-beam (Ar+ polisher) to prepare a site-specific TEM sample by FIB. The TEM sample was characterized by FEI Titan Themis 300 instrument (equipped with a Cs-corrector and 4 quadrant EDX detectors), operated at 300 KV. X-ray computed tomography (diondo d2, GE Company) with microfocus CT detection system was used for visualizing the distribution of diamond particles in the Dia/Gr/Cu composites. The sample was rotated 360 degrees within the detection range and irradiated. Meanwhile, a 2D projection image was acquired for each angle. Then the acquired 2D projection image was reconstructed by computer data to obtain 3D CT volume data. Finally, visual analysis of data was obtained by the dedicated software. To characterize thermal stability, differential scanning calorimetry (DSC) and thermogravimetric analysis (TGA) were conducted on thermal analyser (Netzsch STA449 F3, Germany) from room temperature to 1200 ℃ with a heating rate of 10 ℃/min under dynamic argon atmosphere (purity 99.999%, 20 ml/min). Before measurement, the baseline was calibrated at a heating rate of 10 ℃/min using two empty alumina crucibles. During the measurement, the composite was loaded in an alumina crucible with another empty alumina crucible used for reference. Specimens for compression testing were manufactured as cylinders with a size of Ø 3 × 3.5 mm. The compression test was carried out at 298 K and the loading rate was 0.18 mm/min.

2.5. Thermal Conductivity Measurements

The TC of the composites was calculated according to $\kappa = \alpha \times \rho \times C_p$. Thermal diffusivity (α) and specific capacity (C_p) of the sintered composites were measured by a laser flash method on a Netzsch LFA 427 at room temperature (298 K). The sample density (ρ) was examined by the Archimedes method. The samples (Ø 12.7 × 3 mm) were coated with a graphite coating using a carbon spray on the top and bottom surfaces to improve the capability of the sample to absorb the energy applied. Five parallel positions were measured to obtain an average TC value for each sample. The temperature dependency of TC of the composites were measured between the temperatures of 298 to 573 K.

2.6. Time-domain thermoreflectance (TDTR) Measurements

The TDTR is an optical pump-probe method for measuring interfacial thermal conductance. A schematic diagram of TDTR measurement system is shown in **Fig. S2** (Supporting Information). A Ti: sapphire laser generates a train of 140 fs pulses with a frequency of 80 MHz. Then, the laser beam is split into a pump and a probe beam. The pump beam heats the sample surface in a short time, producing periodic heating at the sample surface. The intensity of reflected probe beam on the sample shows the temperature of the sample surface since the reflectivity of the sensing layer is approximately linear with temperature within a certain temperature range. The temperature profile can also be calculated by a thermal model. From the experimental data, we can extract the unknown thermal properties (ITC) by fitting the ratio of the in-phase (V_{in}) and the out-of-phase (V_{out}) voltages (V_{in}/V_{out}, as the measured signals) to a heat transfer model. The TDTR experiments were conducted at five different locations, and each location was scanned three times. The detailed parameters for ITR measurement is shown in **Table S2** (Supporting Information).

3. Results and Discussion

3.1. Characterization of the diamond particles

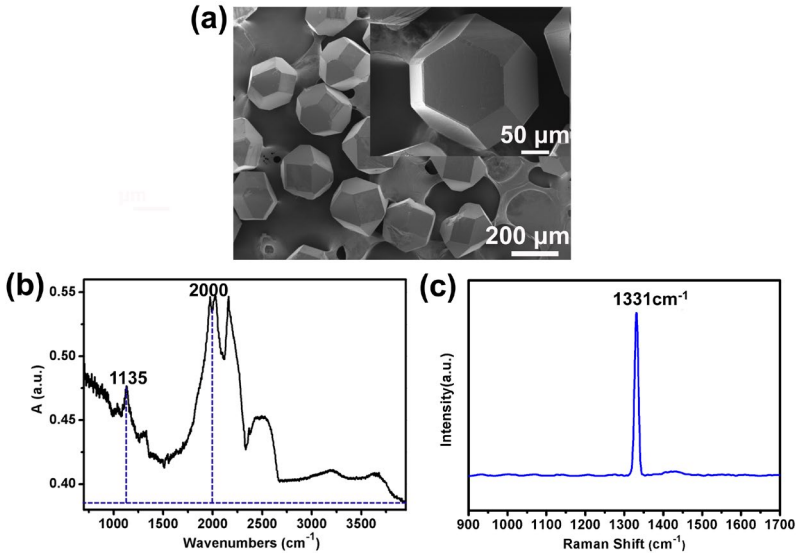

Fig. 2. (a) SEM images of raw diamond, micro FTIR spectra (b) and Raman spectra (c) for the raw diamond particles.

Fig. 2a shows the SEM image of the pristine diamond particles with a mean average size of ~200 μm. The κ (TC) of diamond with tetrakaidecahedron morphology synthesized by high pressure high temperature (HPHT) is mainly dominated by nitrogen concentration (Nc) **[5, 6, 39]**, which can be derived by the absorption peaks at 1135 and 2000 cm^{-1} in FTIR spectrum, as shown in **Fig. 2b**. The corresponding formula is shown as **[6]** :

$$Nc\ (ppm) = 308\ A(1135\ cm^{-1}) / A(2000\ cm^{-1}) \quad (1)$$

where A(1135 cm^{-1}) and A(2000 cm^{-1}) represent the relative absorption coefficients at 1135 and 2000 cm^{-1}, respectively. The Nc is determined to be 180 ppm according to **Eq. (1)**. The κ of diamond particle is estimated to be 1600 W/mK from the relationship between κ and Nc **[5]**:

$$\kappa = 2200 - 3.27\ Nc \quad (2)$$

The representative peak detected at 1331cm^{-1} in Raman spectra (**Fig. 2c**) confirms the structure of diamond.

3.2. Characterization of the Gr/Cu powders and in situ grown graphene

The pristine copper powders present a smooth surface as shown in **Fig. 3a**. The composition are shown in **Fig. S3** and **Table S3** (Supporting Information). Small amounts of other impurity elements (Al, Si, Fe, Pb, Sn, Zn) are detected in the raw Cu powders. Relatively transparent graphene with some wrinkles are uniformly covered on Cu particles (**Fig. 3b**). Moreover, graphene with various thickness can be obtained on the spherical Cu particles by adjusting the concentration of carbon source, as seen from the TEM images of bulk graphene/copper (Gr/Cu) composites (**Fig. S4**, Supporting information), which was prepared through the same method. To further investigate the as-grown graphene, we etched the Cu substrate with $FeCl_3$ solution. SEM (**Fig. S5,** Supporting Information) and TEM (**Fig. 3c**) images depict the typical morphology of graphene. Higher magnification image displays the typical crystalline graphene lattice (inserted image in **Fig. 3c**). In Raman spectra (**Fig. 3d**), the representative *D*, *G* and 2*D* peaks were detected at 1342 cm^{-1}, 1574 cm^{-1} and 2673 cm^{-1}, respectively. The three peaks confirm graphene structure. Red shifts (peaks positions shift to

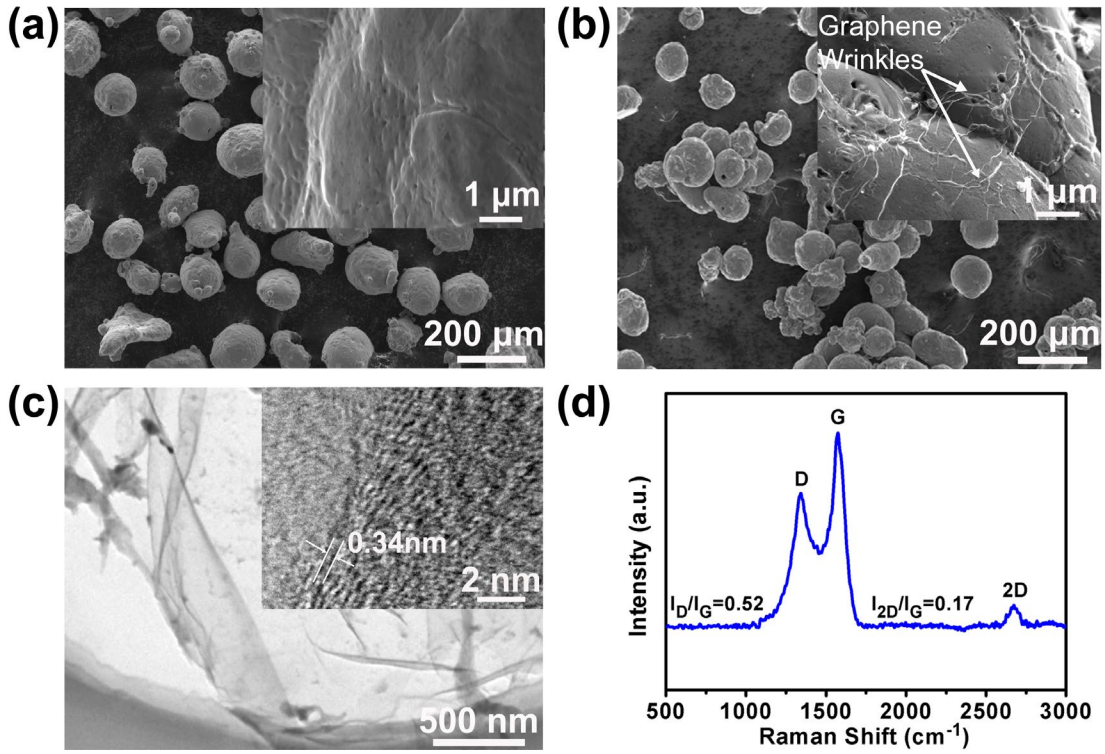

Fig. 3. (a) SEM images of copper powders and (b) in situ grown Gr/Cu. The insets show their surface morphologies at a higher magnification; (c) TEM images at lower and (inset) higher magnifications of the in situ grown graphene; (d) Raman spectra of the as grown graphene obtained from Gr/Cu powders by $FeCl_3$ solution etching.

lower frequency) on the D and G peaks (compared with the representative peaks positions at 1580 cm^{-1} and 2680 cm^{-1}, respectively) **[40]** are observed for the obtained graphene. This effect is related to strain in graphene, produced from the laser power, contacting substrate and internal strain during the Raman test **[41]**. In the composites, the externally applied pressure would introduce internal stress in graphene during the sintering process. The possible strain may decrease the intrinsic thermal conductivity of the graphene **[28]**. A low ratio I_D/I_G (~0.52 ± 0.04) demonstrate the graphene possesses a low defect density **[38]**. The density of defects in graphene, N_D, can also be quantified according to the following equation **[28]**:

$$N_D\left(cm^{-2}\right) = \frac{(1.8 \pm 0.5) \times 10^{22}}{\lambda^4} \left(\frac{I_D}{I_G}\right) \qquad (3)$$

where λ is the laser wave length. The defect density increases linearly with the ratio of I_D/I_G, and the N_D values of the as-prepared graphene are calculated to be $11.73 \pm 3.26\times10^{10}$ cm^{-2}. Furthermore, in comparison with that of single layer graphene ($I_{2G}/I_D = 2$) **[41]**, the relatively low I_{2G}/I_D (~0.17 ± 0.02) value illustrates that multilayer graphene is obtained.

3.3. Characterization of bulk Dia/Gr/Cu composites

Backscattered electron images **(Fig. 4a,b)** of the fractured surface for Dia/Cu composite without graphene show that large amounts of wide gaps (marked in **Fig. 4a)** are obviously observed around diamond particles as well as some small and spherical Cu particles were accumulated on the diamond surface (**Fig. 4b)**, suggesting poor wettability and possible weak bonding between copper and diamond. Interface debonding occurs when the Dia/Cu composite is broken. As shown in **Fig. 4c,** no observable voids or gaps can be seen in the Dia/Gr/Cu composite. Diamond particles show close contacts with Cu matrix (**Fig. 4d and**

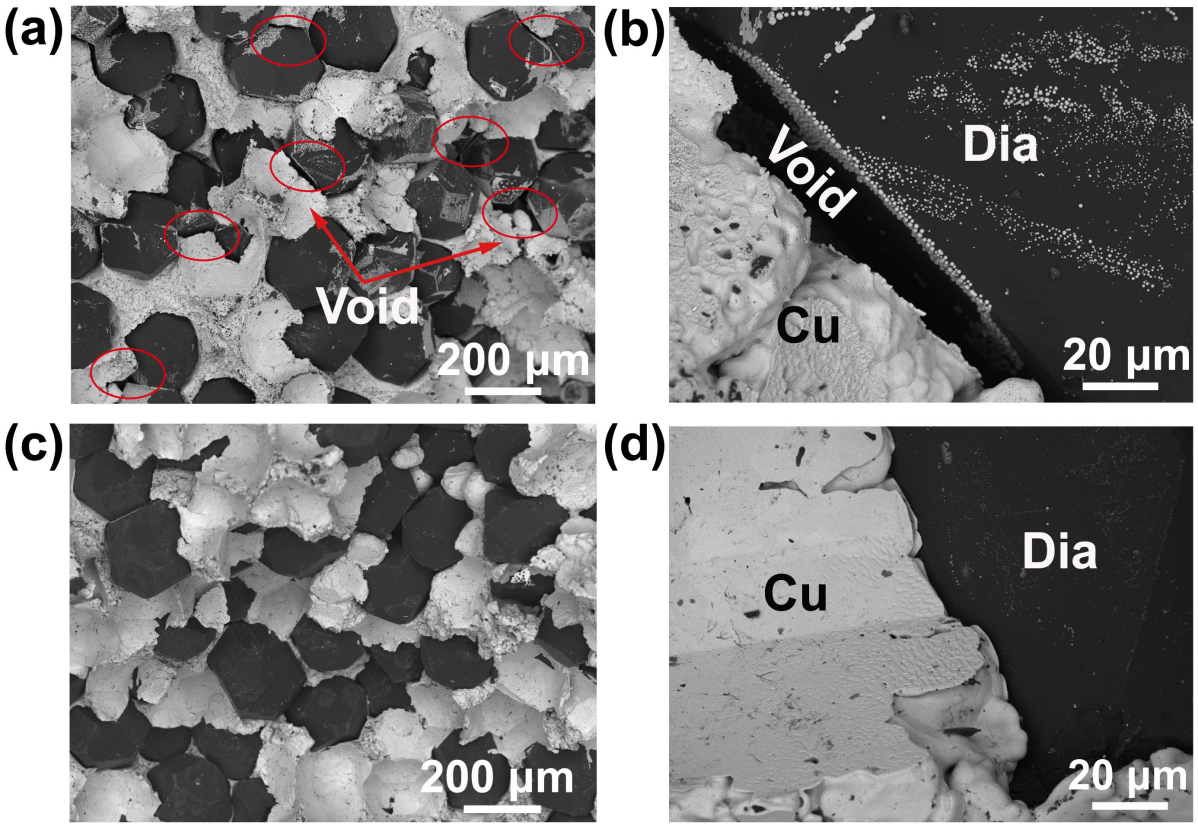

Fig. 4. SEM images for the fractured surface of (a,b) Dia/Cu and (c,d) Dia/Gr/Cu composites.

Fig. S6, Supporting information) in comparison to Dia/Cu composite. When the sintering temperature is 1223 K, the Dia/Gr/Cu composite displays a high relative density of 98.6% (**Fig. S7**, Supporting information). The void fractions in Dia/Cu composite and Dia/Gr/Cu composite are 5.4 vol.% and 1.4 vol.%, respectively. Therefore, the promoted wettability between diamond particles and copper matrix contributed to the densification of Dia/Cu composite after introduction of graphene. XRD patterns in **Fig. S8** (Supporting information) show the existence of diamond and Cu in Dia/Gr/Cu composite. No peaks of graphene are detected because of a low content of graphene in the composite. The strain-stress curves indicate that the compressive strength of the Dia/Gr/Cu composite is ~310 MPa, which is higher than that of Dia/Cu counterpart (**Fig. S9,** Supporting information). Three-dimensional X-ray computed tomography (3D CT) was adopted to visualize distribution of diamond particles in the Dia/Gr/Cu composite. As shown in both the two-dimensional (2D) **(Fig. 5a)** and three-dimensional (3D) **(Fig. 5b)** figures, diamond particles with similar sizes are uniformly distributed in the Cu matrix, creating a condition for homogenously thermal conduction in the composites.

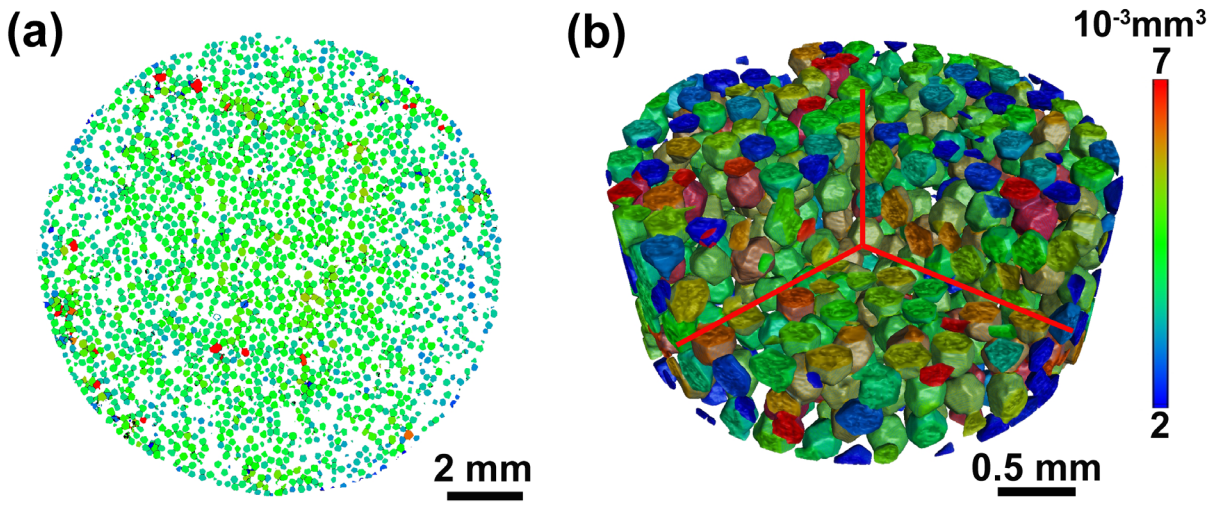

Fig. 5. (a) 2D and (b) 3D images for the distribution of diamond particles in the Dia/Gr/Cu composite with 50 vol.% diamond characterized by three-dimensional X-ray computed tomography.

3.4. Interface structure of bulk Dia/Gr/Cu composites

Interface structure of the Dia/Gr/Cu composite sample with 0.1 vol.% graphene was characterized by TEM. Phase composition of the composited structure is figured out. As labelled in **Fig. S10** (supporting information), the composite consists of three distinct regions of Cu, interlayer and diamond filler. Smooth and clear interface between Cu and diamond is observed (**Fig. 6a**). Close bonding between diamond and Cu was achieved by incorporation of in situ grown graphene. Based on the high resolution TEM image (**Fig. 6b**), the interlayer between diamond and Cu is identified as graphene layers, and fringes of multi layers graphene are observed in the interface layers. The thickness of graphene layers is about ~10 nm. Owing to the in situ growth of graphene on Cu, non-uniform interlayer thickness can be avoided. According to the fractured surface (**Fig. 4c,d)** and TEM results (**Fig. 6b**), we can conclude that a thin graphene layers exist in the interlayer. The existence of in-situ grown nano-graphene interlayer can prevent direct contacts between the diamond particle and Cu matrix, and thus the interface compatibility and interface combination between Cu and diamond are improved, which contributes to the high TCs of the Dia/Gr/Cu composites.

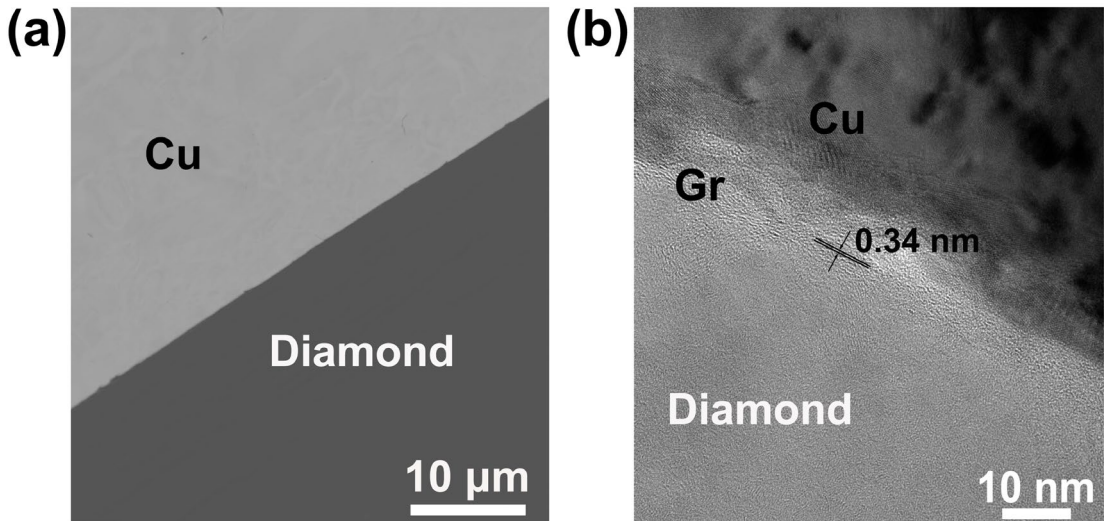

Fig. 6. (a) SEM image for the ion-beam polished surface of Dia/Gr/Cu and (b) TEM images of the Dia/Gr/Cu interface.

3.5. Thermal Properties of the Dia/Gr/Cu Composites

The detailed parameters of thermal conduction for the tested samples are shown in **Table S4** (Supporting Information), including density, thermal diffusivity, specific heat and as-calculated thermal conductivity. Thermal conductivity (κ) and thermal diffusivity (α) of the composites are shown in **Fig. 7a**. The pure Cu sample has a little bit lower TC (359.2 W/mK) than the standard value (~390 W/mK) due to existence of voids and pores. After addition of diamond, TC of the Dia/Cu composite (355.2 W/mK) even decreases and is much lower than the theoretical value calculated from Maxwell model **[42]** because of poor wettability and weak interface bonding between diamond and Cu, which leads to a low ITC. The high porosity with a relative density of 94.8% degrades TC of Dia/Cu composite. Compared with the thermal conductivity from **Fig.7**, all the Dia/Gr/Cu composites show higher thermal conductivities than that of Dia/Cu composite (342.12 ± 5.91 W/mK) without graphene layer. So the graphene can act as an effective interlayer to improve the thermal conductivity of Dia/Cu composite. Different content of graphene lead to various thermal conductivities of Dia/Gr/Cu composites. With adjusting the content of graphene, TC of the bulk Dia/Gr/Cu

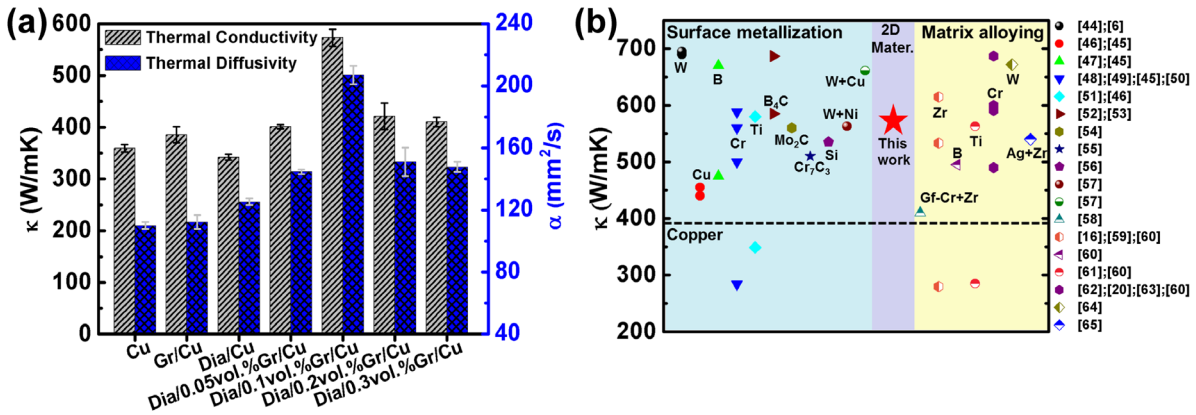

Fig. 7. (a) Thermal conductivity and thermal diffusivity of Dia/Cu, Gr/Cu and Dia/Gr/Cu composites; (b) Comparison on TC with the reported data for the 50 vol.% Dia/Cu composites prepared by the methods of surface metallization on diamond or matrix alloying.

composite firstly increases and then decreases, giving the highest κ of 572.9 W/mK with 0.1 vol.% graphene modification. Prepared by the same method, Gr/Cu composite was almost be fully densified. Without voids and pores, the densified Gr/Cu composite possesses a thermal conductivity close to standard value (~390 W/mK) of Cu. However, with addition of diamond particles, a low content graphene cannot cover the whole interface. Therefore, the problem of poor wetting and thus voids was partially addressed by such nonuniform interlayer in the Dia/0.05 vol.% Gr/Cu composite, leading to a TC slightly higher than that of Gr/Cu sample. The dependence of TC on graphene content is interpreted as follows. On the one hand, too low content of graphene leads to uncoated Cu particles and discontinuous interface, triggering to large voids and a low TC. With increasing graphene content from 0 to 0.1 vol.%, the cover area of graphene on the interface increases and avoids direct contacts of Cu and diamond, leading to the decrease of de-wetting area and resulting in high density and few voids. On the other hand, with increasing graphene content from 0.1 to 0.2 vol.%, the decreased TC of the composite is due to the decreased ITC, which can be expressed as **[43]** :

$$1/G = 1/G_{Cu/Gr} + \frac{d}{\kappa_{Gr}} + 1/G_{Gr/\mathrm{Dia}} \qquad (4)$$

where G, $G_{Cu/Gr}$, $G_{Gr/Dia}$ are the ITC of composite, Cu/Gr and Gr/diamond, respectively. The d and κ_{Gr} are the thickness of graphene layer and thermal conductivity of graphene, respectively. The term d/κ_{Gr} contributes to the ITC of composites largely. As suggested by **Eq. (4)**, the interlayer should be as thin as possible in order to maximize the ITC. Too thick graphene is adverse for improving the thermal conductivity of the Dia/Gr/Cu composites, which is similar to the carbide interlayer in the strategies of surface metallization and matrix alloying. Accordingly, with increasing graphene content from 0.1 vol.% to 0.2 vol.%, the TC decreases from 572.9 to 421.2 W/mK. The TC (410.28 ± 9.11 W/mK) of Dia/0.3 vol.% Gr/Cu composite continues the degrading tendency. The high TC obtained at the intermediate content of graphene layer is a compromise between two competing factors: the improved

interface wetting and the maximized ITC. Temperature dependency of thermal conductivity for Dia/Gr/Cu composites is shown in **Fig. S11** (Supporting Information). The TC of the composites decreases with increasing temperature. Dia/0.1vol.%Gr/Cu composite still exhibits higher TC than those of the other samples at elevated temperatures. Results of DSC and TGA measurements are shown in **Fig. S12** (Supporting Information). With increasing temperature, the TG curve of the Dia/Gr/Cu composite stay at a nearly constant value, indicating its highly thermal stability.

As compared in **Fig. 7b**, with ~50 vol.% diamond, the obtained TC of 572.9 W/mK is comparable to the reported values of that prepared by surface metallization on diamond **[6, 44-57]** and Cu-X alloy matrix (X refer to carbide forming element) **[16, 20, 58-65]**, and even higher than some results. As compared to those higher reported data **[16, 44, 52, 57]**, the thermal conductivity of our Dia/Gr/Cu composites could be further improved by considering the following factors. Firstly, scanning transmission electron microscopy – high angle annular dark field (STEM – HAADF) imaging indicates that oxides contaminants exist near the Dia/Gr/Cu interface (**Fig. S13**, supporting information), which is expected to be removed at stronger reducing conditions. And also the quality of graphene can be further improved by optimizing reducing and growing conditions. Secondly, the relative density (~98.6%) could be further enhanced by hot-pressing process at higher pressure and higher temperature **[16]**. Additionally, as predicted by Maxwell **[42]**, H-J model **[66]** and differential effective medium (DEM) **[67]**, larger diamond particle size is beneficial for enhancing thermal conductivity of composites, and diamond with larger diameter can be used (such as ~300 μm **[64]**).

In particular, as an individual filler, neither graphene nor diamond significantly improves the TC of Cu matrix composites. After interface modification by in-situ grown graphene between diamond and Cu, the bulk Dia/Gr/Cu composites exhibit higher TCs than that of both Gr/Cu and Dia/Cu composite. As the interlayer, in-situ grown graphene plays a dominate role in the enhancing TC. First, surface energies of diamond and graphene are 45.6 mJ/m^2 **[31]** and

46.7 mJ/m^2 **[32]**, respectively. With similar surface energy, as its allotrope, the graphene has good chemical affinity with the diamond and avoids directly contacts between Cu and diamond under high temperature. Second, the in-situ growth of graphene on Cu particles and sintering process provides a strong interface bonding between graphene and Cu. Hwang et al. **[30]** confirmed that the sintered graphene and Cu showed a high adhesion energy of 164 J/m^2. Additionally, the hybrid interface between diamond and graphene may provide a stable bonding **[68]**, which leads to a lower ITR (interfacial thermal resistance). The ITR between diamond and graphene calculated by Shiga et al. **[69]** was 1.43×10^{-10} m^{2}K/W, which was about two orders of magnitude smaller than those of the weakly (van der Waals) bonded interface between graphene and underlying substrate obtained by experiments **[70]**.

3.6. Interfacial Thermal Conductance of Dia/Gr/Cu Composites

Electron and phonon are the main heat carriers in metal and in diamond, respectively. Scattering and electron-phonon interactions at the interface determine the TC of diamond/metal composites by affecting the ITC **[71]**. For the in-situ grown graphene itself, acoustic impedance (Z) and the thickness make it play a similar role in Dia/Cu composites compared to carbide introduced by surface metallization and matrix alloying. According to

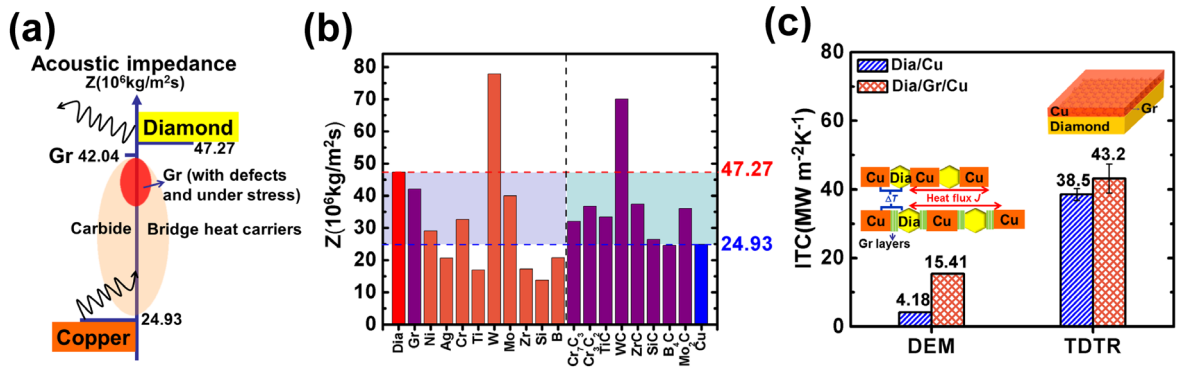

Fig. 8. (a) Acoustic impedance difference between diamond and Cu; (b) Comparison on reported acoustic impedance of metal coating and carbide **[72]**; (c) Results of ITC obtained from DEM calculations of the bulk Dia/Gr/Cu composite and from TDTR measurement of Dia/Gr/Cu model specimens.

the theory of acoustic mismatch model (AMM), the ITC strongly depends on the phonon transmission coefficient. Interlayer with an intermediate Z provides a higher phonon transmission coefficient than that without any interlayer. Therefore, Z of the interlayer is the decisive factor of ITC. A reasonable interface modification layer should be able to balance the effect of acoustic impedance between diamond and Cu as shown in **Fig. 8a**. At present, Z values of the commonly used carbide interlayers (data from Yuan et al. **[72]**, as shown in **Fig. 8b**) are mostly between diamond and Cu matrix **[8]**. Although Z of pristine graphene (Z_{Gr} = 42.04 × 10^6 kg/m^2s **[34])** is only slightly lower than the value of diamond, defects and stress suppress phonon velocity of graphene **[35-37]**, and thus the Z of the in-situ grown graphene ($I_D/I_G \approx 0.52$) should be less than 42.04 × 10^6 kg/m^2s. Therefore, graphene is an appropriate interlayer for interface modification and bridging the vibrational mismatch of phonons between diamond and Cu.

From theoretical model, the thickness of carbide as small as possible showed a positive effect for improving TC and ITC **[48]**. However, the optimum thickness of the carbide transition layers was confined to the 50~200 nm interval **[24, 62, 73-75]** for increasing the ITC. Preferential bonding of carbide on crystal faces of diamond was confirmed by previous studies **[12, 19-23]**. Preferential bonding **[12, 20, 21, 23]** and different growth rate of carbide **[19, 22]** on {100} face and {111} face of diamond gave rise to nonuniform thickness of interlayers. In order to obtain overall coverage of carbide interlayers on all the crystal faces of diamond particles, the thickness of the carbide interlayers on the preferred crystal face obtained from surface metallization or matrix alloying were too thick (usually > 200 nm). However, too thick carbide layers impaired interfacial heat transfer because carbide layers themselves had lower TCs than those of the diamond filler (1500 W/mK) and of the matrix (390 W/mK for Cu) **[75]**. The maximum possible TC value will be attained for the condition of a thin and continuous carbide layer. Therefore, the optimized value of real thickness for the

metallic carbide may be <100 nm. In-situ grown graphene layers whose thickness is less than 50 nm is appropriate for interface modification.

As shown in **Fig. 8c,** the ITC is estimated by theoretical calculation from DEM model **[67, 76, 77]** and by experimental measurement from time-domain thermoreflectance (TDTR) on the model materials (the detailed description are shown in **S16**, Supporting Information)**.** DEM is widely used for analysis of thermal conductivity of Dia/Cu composites with high content of diamond. The expression for DEM model is

$$\left(1\text{-}V_{\mathrm{d}}\right)\left(\frac{\kappa_c}{\kappa_m}\right)^{\frac{1}{3}}=\frac{\kappa_d^{eff}-\kappa_c}{\kappa_d^{eff}-\kappa_m} \qquad (5)$$

$$\kappa_d^{eff}=\frac{\kappa_d}{1+\frac{\kappa_d}{aG}} \qquad (6)$$

where κ refers to the thermal conductivity, V is the volume fraction of diamond particles, a presents the average radius of diamond particles and G is the interfacial thermal conductance (ITC) between matrix and reinforcement particles. Subscripts *m, d* and *c* refer to Cu matrix, diamond particles and the composite, respectively. κ_d^{eff} is the effective TC of diamond. From the **Eq. (5)**, we obtained the κ_d^{eff} , then the G can be deduced from following equation,

$$G=\frac{\kappa_d^{eff}}{\kappa_d\text{-}\kappa_d^{eff}}\cdot\frac{\kappa_d}{a} \qquad (7).$$

As estimated from SEM and TEM, the fraction of graphene is limited. With modification of graphene on Cu, κ_m = 380 W/mK, κ_c = 572.9 W/mK, κ_d = 1600 W/mK and a is 100 μm. According to the **Eq. (7),** the value of ITC of Dia/Cu composite without graphene is calculated to be 4.18 MW/m^{2}K. With incorporating the graphene interlayer, all the Dia/Gr/Cu composites show higher ITC, and the ITC of the Dia/Gr/Cu composites with 0.05 vol.% Gr, 0.2 vol.% Gr and 0.3 vol.% Gr were increased to the values of 5.76 MW/m^{2}K, 6.56 MW/m^{2}K and 6.11 MW/m^{2}K, respectively. Especially, the optimized volume fraction of graphene of 0.1

vol.% led to a 3.7 times enhancement of ITC, indicating the graphene interlayer can effectively improve the ITC between diamond and Cu. Furthermore, the TDTR method was used to measure the ITC between diamond and Cu from the model materials. From the experimental results, we can see that the ITC increases from 38.5 MW/m^2K to 43.2 MW/m^2K due to introduction of graphene at the interface between diamond and Cu. Due to the porosity and quality of graphene, the calculated value is lower than measured value. However, it has to be mentioned that the larger disparity of ITC from calculation is based on the in-situ growth of graphene on Cu instead of the transferred graphene in model material and also densification by hot pressing process of bulk Dia/Gr/Cu composite, which provides a stronger bonding between Cu and diamond. But the role of graphene is confirmed by both DEM calculation and TDTR experiment. In Dia/Cu system, the disorder state **[78]** and adhesion **[78, 79]** between diamond and Cu affected ITC. A lower level of disorder resulted from a lower nitrogen content in diamond, and stronger adhesion arouse from transition metals interlayers between diamond and Cu would increase the ITC **[78, 79]**. As the interlayer, graphene may improve the adhesion between the diamond and Cu, resulting in a higher ITC. Therefore, the TC improvement is mainly attributed to the increase of ITC and bridging vibrational mismatch of phonons between diamond and Cu.

4. Conclusions

In summary, a novel interface modification approach is proposed to improve ITC of the Dia/Cu composites beyond the widely adopted methods of surface metallization and matrix alloying, by which nano-sized thick and uniform graphene layer is introduced at the interface. This approach avoids the challenges that met in the methods of surface metallization and matrix alloying, such as growing uniform carbide nanolayer and TC degradation of alloy matrix. The in situ grown graphene on Cu particle surface has good bonding with Cu matrix as well as good compatibility with its allotrope of diamond. Moreover, graphene has well phonon match with diamond and copper, and also has a much higher intrinsic thermal

conductivity than carbides. As compared to the Dia/Cu counterpart, the introduction of graphene interlayer leads to ~4 folds increase on interface thermal conductance and >60% enhancement on thermal conductivity. The strategy could be also expanded to other 2-D materials and other metal matrix composites, for example, encapsulating diamond or metal particles with MXene phases (2-D nanomaterials of transitional metal carbides or nitrides) **[80, 81]**. This work provides a simple but very effective strategy to fabricate high performance metal matrix composites for thermal management applications.

Acknowledgments

This work was supported by the National Key R&D Program of China (No.2017YFB0406200), the National Natural Science Foundation of China (Nos. 51771110, 51371115, 51671130, 51771111), the Shanghai Science & Technology Committee (Nos. 15JC1402100, 17520712400), the Ministry of Science & Technology of China (No. 2016YFE0130200).

References

[1] Q.Y. Zheng, S. Li, C.H. Li, Y.C. Lv, X.Y. Liu, P.Y. Huang, D.A. Broido, B. Lv, D.G. Cahill, High Thermal Conductivity in Isotopically Enriched Cubic Boron Phosphide, Adv. Funct. Mater. 28 (2018) 1805116.

[2] S. Li, Q.Y. Zheng, Y.C. Lv, X.Y. Liu, X.Q. Wang, P.S.E.Y. Huang, D.G. Cahill, B. Lv, High thermal conductivity in cubic boron arsenide crystals, Science 361 (2018) 579-581.

[3] J.S. Kang, M. Li, H.A. Wu, H. Nguyen, Y.J. Hu, Experimental observation of high thermal conductivity in boron arsenide, Science 361 (2018) 575-578.

[4] J. Anaya, S. Rossi, M. Alomari, E. Kohn, L. Toth, B. Pecz, K.D. Hobart, T.J. Anderson, T.I. Feygelson, B.B. Pate, M. Kuball, Control of the in-plane thermal conductivity of ultra-thin nanocrystalline diamond films through the grain and grain boundary properties, Acta Mater. 103 (2016) 141-152.

[5] Y. Yamamoto, T. Imai, K. Tanabe, T. Tsuno, Y. Kumazawa, N. Fujimori, The measurement of thermal properties of diamond, Diam. Relat. Mater. 6 (1997) 1057-1061.

[6] A.M. Abyzov, M.J. Kruszewski, L. Ciupinski, M. Mazurkiewicz, A. Michalski, K.J. Kurzydlowski, Diamond-tungsten based coating-copper composites with high thermal conductivity produced by Pulse Plasma Sintering, Mater. Des. 76 (2015) 97-109.

[7] F. Delannay, L. Froyen, A. Deruyttere, The wetting of solids by molten metals and its relation to the preparation of metal-matrix composites composites, J. Mater. Sci. 22 (1987) 1-16.

[8] G. Chang, F. Sun, J. Duan, Z. Che, X. Wang, J. Wang, M.J. Kim, H. Zhang, Effect of Ti interlayer on interfacial thermal conductance between Cu and diamond, Acta Mater. 160 (2018) 235-246.

[9] S. Ren, J. Chen, X. He, X. Qu, Effect of matrix-alloying-element chromium on the microstructure and properties of graphite flakes/copper composites fabricated by hot pressing sintering, Carbon 127 (2018) 412-423.

[10] G.Z. Bai, N. Li, X.T. Wang, J.G. Wang, M.J. Kim, H.L. Zhang, High thermal conductivity of Cu-B/diamond composites prepared by gas pressure infiltration, J. Alloy. Compd. 735 (2018) 1648-1653.

[11] J.W. Li, H.L. Zhang, L.H. Wang, Z.F. Che, Y. Zhang, J.G. Wang, M.J. Kim, X.T. Wang, Optimized thermal properties in diamond particles reinforced copper-titanium matrix composites produced by gas pressure infiltration, Compos. Part A 91 (2016) 189-194.

[12] H. Chen, C.C. Jia, S.J. Li, X. Jia, X. Yang, Selective interfacial bonding and thermal conductivity of diamond/Cu-alloy composites prepared by HPHT technique, Int. J. Min. Met. Mater. 19 (2012) 364-371.

[13] J.S. He, H.L. Zhang, Y. Zhang, Y.M. Zhao, X.T. Wang, Effect of boron addition on interface microstructure and thermal conductivity of Cu/diamond composites produced by high temperature-high pressure method, Phys. Status Solidi A 211 (2014) 587-594.

[14] Y. Pan, X. He, S. Ren, M. Wu, X. Qu, Optimized thermal conductivity of diamond/Cu composite prepared with tungsten-copper-coated diamond particles by vacuum sintering technique, Vacuum 153 (2018) 74-81.

[15] A.M. Abyzov, S.V. Kidalov, F.M. Shakhov, High thermal conductivity composite of diamond particles with tungsten coating in a copper matrix for heat sink application, Appl. Therm. Eng. 48 (2012) 72-80.

[16] K. Chu, C.C. Jia, H. Guo, W.S. Li, On the thermal conductivity of Cu-Zr/diamond composites, Mater. Des. 45 (2013) 36-42.

[17] T. Schubert, L. Ciupinski, W. Zielinski, A. Michalski, T. Weissgaber, B. Kieback, Interfacial characterization of Cu/diamond composites prepared by powder metallurgy for heat sink applications, Scripta Mater. 58 (2008) 263-266.

[18] D.A. Mortimer, M. Nicholas, The wetting of carbon and carbides by copper alloys, J. Mater. Sci. 8 (1973) 640-648.

[19] J. Grzonka, M.J. Kruszewski, M. Rosinski, L. Ciupinski, A. Michalski, K.J. Kurzydlowski, Interfacial microstructure of copper/diamond composites fabricated via a powder metallurgical route, Mater. Charact. 99 (2015) 188-194.

[20] L. Weber, R. Tavangar, On the influence of active element content on the thermal conductivity and thermal expansion of Cu-X (X = Cr, B) diamond composites, Scripta Mater. 57 (2007) 988-991.

[21] H. Chen, C.C. Jia, S.J. Li, Interfacial characterization and thermal conductivity of diamond/Cu composites prepared by two HPHT techniques, J. Mater. Sci. 47 (2012) 3367-3375.

[22] H.D. Zhang, J.J. Zhang, Y. Liu, F. Zhang, T.X. Fan, D. Zhang, Unveiling the interfacial configuration in diamond/Cu composites by using statistical analysis of metallized diamond surface, Scripta Mater. 152 (2018) 84-88.

[23] J. Flaquer, A. Rios, A. Martin-Meizoso, S. Nogales, H. Bohm, Effect of diamond shapes

and associated thermal boundary resistance on thermal conductivity of diamond-based composites, Comp. Mater. Sci. 41 (2007) 156-163.

[24] L. Wang, J. Li, M. Catalano, G. Bai, N. Li, J. Dai, X. Wang, H. Zhang, J. Wang, M.J. Kim, Enhanced thermal conductivity in Cu/diamond composites by tailoring the thickness of interfacial TiC layer, Compos. Part A 113 (2018) 76-82.

[25] Z. Tan, Z. Chen, G. Fan, G. Ji, J. Zhang, R. Xu, , A. Shan, Z. Li, D. Zhang, Effect of particle size on the thermal and mechanical properties of aluminum composites reinforced with SiC and diamond, Mater. Des. 90 (2016) 845-851.

[26] E. Mohammad Sharifi, F. Karimzadeh, M.H. Enayati, Fabrication and evaluation of mechanical and tribological properties of boron carbide reinforced aluminum matrix nanocomposites, Mater. Des. 32 (2011) 3263-3271.

[27] A.A. Balandin, S. Ghosh, W.Z. Bao, I. Calizo, D. Teweldebrhan, F. Miao, C.N. Lau, Superior thermal conductivity of single-layer graphene, Nano Lett. 8 (2008) 902-907.

[28] H. Cao, D.-B. Xiong, Z. Tan, G. Fan, Z. Li, Q. Guo, Y. Su, C. Guo, D. Zhang, Thermal properties of in situ grown graphene reinforced copper matrix laminated composites, J. Alloy. Compd. 771 (2019) 228-237.

[29] Y.K. Chen, X. Zhang, E.Z. Liu, C.N. He, C.S. Shi, J.J. Li, P. Nash, N.Q. Zhao, Fabrication of in-situ grown graphene reinforced Cu matrix composites, Sci. Rep. 6 (2016) 19363-19371.

[30] J. Hwang, T. Yoon, S.H. Jin, J. Lee, T.S. Kim, S.H. Hong, S. Jeon, Enhanced Mechanical Properties of Graphene/Copper Nanocomposites Using a Molecular-Level Mixing Process, Adv. Mater. 25 (2013) 6724-6729.

[31] L. Ostrovskaya, V. Perevertailo, V. Ralchenko, A. Saveliev, V. Zhuravlev, Wettability of nanocrystalline diamond films, Diam. Relat. Mater. 16 (2007) 2109-2113.

[32] S.R. Wang, Y. Zhang, N. Abidi, L. Cabrales, Wettability and Surface Free Energy of Graphene Films, Langmuir 25 (2009) 11078-11081.

[33] A. Kozbial, Z.T. Li, C. Conaway, R. McGinley, S. Dhingra, V. Vahdat, F. Zhou, B. D'Urso, H.T. Liu, L. Li, Study on the Surface Energy of Graphene by Contact Angle Measurements, Langmuir 30 (2014) 8598-8606.

[34] K. Jagannadham, Thermal Conductivity of Copper-Graphene Composite Films Synthesized by Electrochemical Deposition with Exfoliated Graphene Platelets, Metall. Mater. Trans. B 43 (2012) 316-324.

[35] X. Mu, X. Wu, T. Zhang, D.B. Go, T. Luo, Thermal transport in graphene oxide--from ballistic extreme to amorphous limit, Sci. Rep. 4 (2014) 3909-3917.

[36] S. Chen, Q. Wu, C. Mishra, J. Kang, H. Zhang, K. Cho, W. Cai, A.A. Balandin, R.S. Ruoff, Thermal conductivity of isotopically modified graphene, Nat. Mater. 11 (2012) 203-207.

[37] X. Shen, X.Y. Lin, J.J. Jia, Z.Y. Wang, Z.G. Li, J.K. Kim, Tunable thermal conductivities of graphene oxide by functionalization and tensile loading, Carbon 80 (2014) 235-245.

[38] M. Cao, D.B. Xiong, Z.Q. Tan, G. Ji, B. Amin-Ahmadi, Q. Guo, G.L. Fan, C.P. Guo, Z.Q. Li, D. Zhang, Aligning graphene in bulk copper: Nacre-inspired nanolaminated architecture coupled with in-situ processing for enhanced mechanical properties and high electrical conductivity, Carbon 117 (2017) 65-74.

[39] Z.Q. Tan, Z.Q. Li, G.L. Fan, X.Z. Kai, G. Ji, L.T. Zhang, D. Zhang, Fabrication of diamond/aluminum composites by vacuum hot pressing: Process optimization and thermal properties, Compos. Part B-Eng. 47 (2013) 173-180.

[40] H. Rho, Y.S. Jang, S. Kim, S. Bae, T.W. Kim, D.S. Lee, J. S. Ha, S. H. Lee, Porous copper-graphene heterostructures for cooling of electronic devices, Nanoscale 9 (2017) 7565-7569.

[41] D. Berman, S. A. Deshmukh, B. Narayanan, S.K.R.S. Sankaranarayanan, Z. Yan, A.A. Balandin, A. Zinovev, D. Rosenmann, A. V. Sumant, Metal-induced rapid transformation of diamond into single and multilayer graphene on wafer scale. Nat. Commun. 7 (2016)

12099.

[42] A. Eucken, Heat Transfer in Ceramic Refractory Materials : Calculation from Thermal Conductivities of Constituents, Fortchg.gebiete Ingenieurw.B3 Forschungsheft 16 (1932) 353-360.

[43] Q.Z. Liang, X.X. Yao, W. Wang, Y. Liu, C.P. Wong, A Three-Dimensional Vertically Aligned Functionalized Multilayer Graphene Architecture: An Approach for Graphene-Based Thermal Interfacial Materials, ACS Nano 5 (2011) 2392-2401.

[44] C. Zhang, R.C. Wang, Z.Y. Cai, C.Q. Peng, N.G. Wang, Low-temperature densification of diamond/Cu composite prepared from dual-layer coated diamond particles, J. Mater. Sci.-Mater. El. 26 (2015) 185-190.

[45] T. Guillemet, J.M. Heintz, B. Mortaigne, Y.F. Lu, J.F. Silvain, Formation of Cu Nanodots on Diamond Surface to Improve Heat Transfer in Cu/D Composites, Adv. Eng. Mater. 20 (2018) 1700894-1700903.

[46] T. Guillemet, P.M. Geffroy, J.M. Heintz, N. Chandra, Y.F. Lu, J.F. Silvain, An innovative process to fabricate copper/diamond composite films for thermal management applications, Compos. Part A 43 (2012) 1746-1753.

[47] H. Bai, D. Dai, J.H. Yu, K. Nishimura, S. Sasaoka, N. Jiang, Architecting boron nanostructure on the diamond particle surface, Appl. Surf. Sci. 292 (2014) 790-794.

[48] S.B. Ren, X.Y. Shen, C.Y. Guo, N. Liu, J.B. Zang, X.B. He, X.H. Qu, Effect of coating on the microstructure and thermal conductivities of diamond-Cu composites prepared by powder metallurgy, Compos. Sci. Technol. 71 (2011) 1550-1555.

[49] W. Cui, H. Xu, J.H. Chen, S.B. Ren, X.B. He, X.H. Qu, Effect of sintering on the relative density of Cr-coated diamond/Cu composites prepared by spark plasma sintering, Int. J. Min. Met. Mater. 23 (2016) 716-722.

[50] K. Chu, Z.F. Liu, C.C. Jia, H. Chen, X.B. Liang, W.J. Gao, W.H. Tian, H. Guo, Thermal conductivity of SPS consolidated Cu/diamond composites with Cr-coated diamond

particles, J. Alloy. Compd. 490 (2010) 453-458.

[51] H.Y. Wang, J. Tian, Thermal conductivity enhancement in Cu/diamond composites with surface-roughened diamonds, Appl. Phys. A-Mater. 116 (2014) 265-271.

[52] Y.H. Sun, L.K. He, C. Zhang, Q.N. Meng, B.C. Liu, K. Gao, M. Wen, W.T. Zheng, Enhanced tensile strength and thermal conductivity in copper diamond composites with B4C coating, Sci. Rep. 7 (2017) 10727-10736.

[53] H.B. Hu, J. Kong, Improved Thermal Performance of Diamond-Copper Composites with Boron Carbide Coating, J. Mater. Eng. Perform. 23 (2014) 651-657.

[54] Q.P. Kang, X.B. He, S.B. Ren, L. Zhang, M. Wu, T.T. Liu, Q. Liu, C.Y. Guo, X.H. Qu, Preparation of high thermal conductivity copper-diamond composites using molybdenum carbide-coated diamond particles, J. Mater. Sci. 48 (2013) 6133-6140.

[55] Q.P. Kang, X.B. He, S.B. Ren, L. Zhang, M. Wu, C.Y. Guo, W. Cui, X.H. Qu, Preparation of copper-diamond composites with chromium carbide coatings on diamond particles for heat sink applications, Appl. Therm. Eng. 60 (2013) 423-429.

[56] C.X. Zhu, C. Wang, J. Lang, Y. Ma, N.G. Ma, Si-Coated Diamond Particles Reinforced Copper Composites Fabricated by Spark Plasma Sintering Process, Mater. Manuf. Process. 28 (2013) 143-147.

[57] C. Zhang, Z.Y. Cai, Y.G. Tang, R.C. Wang, C.Q. Peng, Y. Feng, Microstructure and thermal behavior of diamond/Cu composites: Effects of surface modification, Diam. Relat. Mater. 86 (2018) 98-108.

[58] S.B. Ren, H. Xu, J.H. Chen, X.H. Qu, Effects of Sintering Process on Microstructure and Properties of Flake Graphite-Diamond/Copper Composites, Mater. Manuf. Process. 31 (2016) 1377-1383.

[59] A. Rape, X. Liu, A. Kulkarni, J. Singh, Alloy development for highly conductive thermal management materials using copper-diamond composites fabricated by field assisted sintering technology, J. Mater. Sci. 48 (2013) 1262-1267.

[60] T. Schubert, B. Trindade, T. Weissgarber, B. Kieback, Interfacial design of Cu-based composites prepared by powder metallurgy for heat sink applications, Mater. Sci. Eng. A 475 (2008) 39-44.

[61] C.Y. Chung, M.T. Lee, M.Y. Tsai, C.H. Chu, S.J. Lin, High thermal conductive diamond/Cu-Ti composites fabricated by pressureless sintering technique, Appl. Therm. Eng. 69 (2014) 208-213.

[62] L. Ciupinski, M.J. Kruszewski, J. Grzonka, M. Chmielewski, R. Zielinsk, D. Moszczynska, A. Michalski, Design of interfacial Cr3C2 carbide layer via optimization of sintering parameters used to fabricate copper/diamond composites for thermal management applications, Mater. Des. 120 (2017) 170-185.

[63] V. Sinha, J.E. Spowart, Influence of interfacial carbide layer characteristics on thermal properties of copper-diamond composites, J. Mater. Sci. 48 (2013) 1330-1341.

[64] H. Bai, N.G. Ma, J. Lang, C.X. Zhu, Y. Ma, Thermal conductivity of Cu/diamond composites prepared by a new pretreatment of diamond powder, Compos. Part B-Eng. 52 (2013) 182-186.

[65] A. Rape, A. Kulkarni, B. Bhat, J. Singh, Thermal reliability of copper alloy-diamond composites produced by field-assisted sintering technology, J. Compos. Mater. 50 (2016) 1241-1245.

[66] D.P.H. Hasselman, L.F. Johnson, Effective thermal conductivity of composites with interfacial thermal barrier resistance, J. Compos. Mater. 21 (1987) 508-515.

[67] R. Tavangar, J.M. Molina, L. Weber, Assessing predictive schemes for thermal conductivity against diamond-reinforced silver matrix composites at intermediate phase contrast, Scripta Mater. 56 (2007) 357-360.

[68] O.A. Shenderova, D. Areshkin, D.W. Brenner, Bonding and Stability of Hybrid Diamond/Nanotube Structures, Mol. Simulat. 29 (2003) 259-268.

[69] T. Shiga, S. Konabe, J. Shiomi, T. Yamamoto, S. Maruyama, S. Okada, Graphene-

diamond hybrid structure as spin-polarized conducting wire with thermally efficient heat sinks, Appl. Phys. Lett. 100 (2012) 233101.

[70] Y. Yue, J. Zhang, X. Tang, S. Xu, X. Wang, Thermal transport across atomic-layer material interfaces, Nanotechnol. Rev. 4 (2015) 533-555.

[71] G.T. Hohensee, R.B. Wilson, D.G. Cahill, Thermal conductance of metal-diamond interfaces at high pressure, Nat. Commun. 6 (2015) 6578-6586.

[72] M.Y. Yuan, Z.Q. Tan, G.L. Fan, D.B. Xiong, Q. Guo, C.P. Guo, Z.Q. Li, D. Zhang, Theoretical modelling for interface design and thermal conductivity prediction in diamond/Cu composites, Diam. Relat. Mater. 81 (2018) 38-44.

[73] S.V. Kidalov, F.M. Shakhov, Thermal Conductivity of Diamond Composites, Materials 2 (2009) 2467-2495.

[74] C. Zhang, R.C. Wang, Z.Y. Cai, C.Q. Peng, Y. Feng, L. Zhang, Effects of dual-layer coatings on microstructure and thermal conductivity of diamond/Cu composites prepared by vacuum hot pressing, Surf. Coat. Tech. 277 (2015) 299-307.

[75] A.M. Abyzov, S.V. Kidalov, F.M. Shakhov, High thermal conductivity composites consisting of diamond filler with tungsten coating and copper (silver) matrix, J. Mater. Sci. 46 (2011) 1424-1438.

[76] A.G. Every, Y. Tzou, D.P.H. Hasselman, R. Raj, The effect of particle size on the thermal conductivity of ZnS/diamond composites, Acta Metall. Mater. 40 (1992) 123-129.

[77] J.M. Molina, R. Prieto, J. Narciso, E. Louis, The effect of porosity on the thermal conductivity of Al-12 wt.% Si/SiC composites, Scripta Mater. 60 (2009) 582-585.

[78] V. Sinha, J.J. Gengler, C. Muratore, J.E. Spowart, Effects of disorder state and interfacial layer on thermal transport in copper/diamond system, J. Appl. Phys. 117 (2015) 074305.

[79] C. Monachon, L. Weber, Thermal boundary conductance of transition metals on diamond, Emerg. Mater. Res. 1 (2012) 89-98.

[80] M. Naguib, V.N. Mochalin, M.W. Barsoum, Y. Gogotsi, 25th Anniversary Article:

MXenes: A New Family of Two-Dimensional Materials, Adv. Mater. 26 (2014) 992-1005.

[81] X. Si, F. Chen, Q. Deng, S. Du, Q. Huang, Preparation and Property of MXene/Copper Alloy Composites, J. Inorg. Mater. 33 (2018) 603-608.